International Journal of Nanomedicine

Dovepress
open access to scientific and medical research

Open Access Full Text Article

ORIGINAL RESEARCH

Apoptosis-promoting effect of rituximab-conjugated magnetic nanoprobes on malignant lymphoma cells with CD20 overexpression

This article was published in the following Dove Medical Press journal:
International Journal of Nanomedicine

Lina Song[1,2]
Wei Zhang[3]
Hong Chen[4]
Xizhi Zhang[1]
Haoan Wu[1]
Ming Ma[1]
Zhongqiu Wang[2]
Ning Gu[1]
Yu Zhang[1]

[1]State Key Laboratory of Bioelectronics, Jiangsu Key Laboratory for Biomaterials and Devices, School of Biological Science and Medical Engineering & Collaborative Innovation Centre of Suzhou Nano Science and Technology, Southeast University, Nanjing 210096, People's Republic of China; [2]Department of Radiology, Affiliated Hospital of Nanjing University of Chinese Medicine, Nanjing 210029, People's Republic of China; [3]The Jiangsu Province Research Institute for Clinical Medicine, The First Affiliated Hospital with Nanjing Medical University, Nanjing 210009, People's Republic of China; [4]Department of Gastroenterology, Zhongda Hospital, School of Medicine, Southeast University, Nanjing 210009, People's Republic of China

Correspondence: Ning Gu; Yu Zhang
State Key Laboratory of Bioelectronics, Jiangsu Key Laboratory for Biomaterials and Devices, Collaborative Innovation Center of Suzhou Nano Science and Technology, School of Biological Science and Medical Engineering, Southeast University, 87 Dingjiaqiao, District Gulou, Nanjing 210009, China
Tel +86 25 8327 2496
Email zhangyu@seu.edu.cn; guning@seu.edu.cn

Background: Cancer targeting nanoprobes with precisely designed physicochemical properties may show enhanced pharmacological targeting and therapeutic efficacy. As a widely used commercialized antibody, rituximab has been in clinical use for three decades and has lengthened or even saved thousands of lives. However, many people cannot benefit from rituximab treatment because of drug resistance or side effects.

Methods: In this study, a 13-nm rituximab-conjugated magnetic nanoparticle was developed as a therapeutic nanoprobe targeting CD20 overexpressing malignant lymphoma cells to enhance the treatment effects of rituximab. The magnetic cores (2,3-dimercaptosuccinicacid modified Fe_3O_4 nanoparticles, Fe_3O_4@DMSA) of the nanoprobes with an average diameter of 6.5 nm were synthesized using a co-precipitation method. Rituximab was then conjugated on the surface of Fe_3O_4@DMSA using a cross-linking agent (carbodiimide/N-hydroxysulfosuccinimide sodium salt). Based on theoretical calculations, approximately one antibody was coupled with one nanoparticle, excluding the multivalent antibody effect.

Results: Cell targeting experiments and magnetic resonance (MR) signal and T2 measurements showed that the Fe_3O_4@DMSA@Ab nanoprobes have specific binding affinity for CD20-positive cells. Compared to rituximab and Fe_3O_4@DMSA, Fe_3O_4@DMSA@Ab nanoprobes significantly reduced cell viability and promoted Raji cell apoptosis. Initiating events of apoptosis, including increased intracellular calcium and reactive oxygen species, were observed in nanoprobe-treated Raji cells. Nanoprobe-treated Raji cells also showed the most drastic decrease in mitochondrial membrane potential and Bcl-2 expression, compared to rituximab and Fe_3O_4@DMSA-treated Raji cells.

Conclusion: These results indicate that Fe_3O_4@DMSA@Ab nanoprobes have the potential to serve as MRI tracers and therapeutic agents for CD20-positive cells.

Keywords: CD20-targeted nanoprobes, calcium, reactive oxygen species, ROS, mitochondrial membrane potential, MMP, cell apoptosis

Introduction

Targeted therapy has substantial promise in tumor treatment,[1–4] but its efficacy is limited by the need to deliver the drug or antibody in sufficient quantities to the tumor tissue.[5] Over the past decades, researchers have been studying monoclonal antibodies in the clinical application of cancer.[3,6,7] Monoclonal antibodies such as rituximab targeted against the CD20 antigen on the membrane of B-lymphocytes in B-cell non-Hodgkin's lymphoma (NHL) showed a satisfactory curative effect in the clinical treatment of NHL. Rituximab (trade names Rituxan, MabThera, and Zytux) is a chimeric monoclonal antibody approved by the Food and Drug Administration of the United States in 1997.[6] It has been identified that 48% of B cell lymphoma patients respond to rituximab in

submit your manuscript | www.dovepress.com
Dovepress
http://dx.doi.org/10.2147/IJN.S185458

clinical practice.[7] Rituximab can also enhance the sensitization of lymphoma cells to chemotherapeutic drugs.[8]

Rituximab exhibits multiple anti-NHL activities, including complement-dependent cytotoxicity, antibody-dependent cellular cytotoxicity, growth inhibition, and apoptosis.[3,6,7] It has been shown that after binding with rituximab, CD20 on lipid rafts is redistributed to a large lipid raft domain,[9] known to be a signal transduction center. Subsequent signaling events have been observed in rituximab-treated lymphoma cells in vitro, including downregulation of Bcl-2 levels, activation of the Src family members, and regulation of cellular calcium.[10–12] Rituximab can enhance the sensitization of lymphoma cells to chemotherapeutic drugs.[8,13] Bubien et al[14] demonstrated that transfection of CD20 into some CD20-negative cell lines can induce cytosolic calcium release. Furthermore, Tan et al[15] used a quartz crystal microbalance technique to demonstrate that rituximab induced intake of Ca^{2+} ions by Raji cells. This provides valuable information on CD20 as a calcium ion channel on cell membranes. Daniels et al[16] identified that rituximab binding to CD20 causes disequilibrium of intracellular calcium homeostasis and plays an essential role in the process of rituximab-driven caspase-independent apoptosis. In the long term, rituximab is the first-line therapy for B-cell NHL in clinical practice.

NHL is a heterogeneous group of malignant tumors originating in the lymphatic system,[17] its incidence is rising annually. The incidence rate of lymphoma is 4.2% among the cancer registration areas in China. Both the incidence and mortality of lymphoma were ranked ninth in male population in China in 2013.[18] In addition, there were an estimated 72,240 new cases of NHL and around 20,140 deaths in the United States in 2017,[19] showing little change from those in 2016[20] and 2015.[21] In the European Union, about 93.4/1,000 newly diagnosed cases and 37.9/1,000 patients died due to NHL in 2012.[22] Many patients relapse after combination therapy with rituximab and chemotherapy.[23] It has thus become a great challenge to improve therapeutic approach in NHL.

To date, magnetic nanoparticles and magnetic nanoprobes, as a kind of emerging nanomaterial, have been actively investigated as an application in nanomedicine, including magnetic gene and drug delivery,[24] magnetic resonance imaging (MRI),[24,25] thermal therapy,[24,26] cell labeling,[27,28] and in vitro bio-separation.[24,29] For example, Huh et al[30] successfully conjugated the cancer-targeting antibody, Herceptin, to the surface of superparamagnetic iron oxide to form MRI probes. Their study reveals that targeted detection in a mouse xenograft human cancer model by in vivo MRI is achievable. They then designed and synthesized manganese-doped iron oxide nanoparticles for conjugation with antibodies.[31] The nanoprobes showed enhanced MRI sensitivity for detection of small tumors in mice in vivo. Chiu et al[32] developed a construct by grafting rituximab molecules onto liposome membranes to enhance its activity. Nevertheless, few studies have used these as theranostic agents in the simultaneous imaging and treatment of NHL. The advantages of magnetic nanoprobes include accurate diagnosis of NHL at an early stage by clinical MRI and enhancement of curative effects.

Here, we successfully prepared 2,3-dimercaptosuccinic acid (DMSA)-modified iron oxide nanoparticles (Fe_3O_4@DMSA) via a simple co-precipitation technique. The nanoprobes (Fe_3O_4@DMSA@Ab) were prepared to target CD20-overexpressing malignant lymphoma cells. CD20-positive Raji cells were selected as the target cell line and CD20-negative K562 cells were chosen as the control. The feasibility of using these nanoprobes as targeted MRI and therapeutic agents was investigated at the cellular level. Cytotoxicity and cellular specificity were evaluated and cell target binding was monitored by measuring MR signal on a clinical 1.5T MRI scanner changes after incubating the nanoprobes at different amounts with CD20-positive Raji cells. CD20 binding after Fe_3O_4@DMSA@Ab treatment can be induced by the short-range interaction of multiple nanoprobes, which can be strengthened in the presence of a magnetostatic field (MF). The mechanism of Raji cell apoptosis induced by Fe_3O_4@DMSA@Ab nanoprobes might be related to CD20 cluster formation, flux of Ca^{2+}, ROS, and mitochondrial damage. Our results demonstrated that Fe_3O_4@DMSA@Ab could target and induce apoptosis in Raji cells by the short-range interaction of multiple nanoprobes with CD20. The current findings have important implications for the optimization of anti-CD20 strategies in the clinical detection and treatment of B-cell NHLs.

Materials and methods

Materials

All reagents and solvents were obtained from commercial suppliers and were used without further purification. Ferric chloride ($FeCl_3 \cdot 6H_2O$), ferrous sulfate ($FeSO_4 \cdot 7H_2O$), ammonium hydroxide (25% $NH_3 \cdot H_2O$), oleic acid (OA) (90%), n-hexane, and acetone were purchased from Shanghai Chemical Reagent Co., Ltd. (Shanghai, China). DMSA was supplied by Shanghai Zhourui Chemical Reagent Co. Ltd. Rituximab was obtained from Hoffman-La Roche Ltd. (Basel, Switzerland). BSA was obtained from Nanjing Bookman Biotechnology Ltd. Carbodiimide (EDC) and N-hydroxysulfosuccinimide sodium salt (sulfo-NHS) were from Sigma-Aldrich Co. (St Louis, MO, USA). The T/B cell

lymphoma immunohistochemical double dye diagnostic kit was manufactured by Fuzhou Maixin Biotechnology Development Co., Ltd. (Fuzhou, China). Acridine orange (AO), ethidium bromide (EB), Cell Counting Kit 2-(2-methoxy-4-nitrophenyl)-3-(4-nitrophenyl)-5-(2,4-disulfophenyl)-2H-tetrazolum monosodium salt (CCK-8), and the BCA kit were purchased from Nanjing KeyGen Biotech Co. Ltd. (Nanjing, China). Fluo3-AM was from Dojindo Laboratories (Kumamoto, Japan). 2,7-dichlorodihydrofluorescein-diacetate (DCFH-DA) and 5,5,6,6-tetrachloro-1,1,3, 3-tetraethylbenzamidazolocarbocyanin iodide (JC-1) were from Beyotime Biotechnology (Haimen, China). Rabbit anti-Bcl-2, Bax, and β-actin antibodies were manufactured by Beijing Biosynthesis Biotechnology Co., Ltd. (Beijing, China). Double-distilled water was produced using an Aquapro water purification machine (EDI1-1001-U; Aquapro, Yiyang, China).

Synthesis of Fe_3O_4@OA and Fe_3O_4@DMSA magnetic nanoparticles

A mixture of $FeCl_3 \cdot 6H_2O$ (28 g) and $FeSO_4 \cdot 7H_2O$ (20 g) in 80 mL distilled water bubbled with nitrogen air was prepared. Then aqueous ammonia solution (40 mL) was added to the mixture rapidly under vigorous stirring at 72°C. OA (9 mL) was dropped into the reaction system after 5 minutes. After 3 hours, the resulting sediment was washed with ethyl alcohol and distilled water until neutrality was achieved. The OA-coated magnetite particles (Fe_3O_4@OA) were dispersed in n-hexane.

DMSA (200 mg) was dissolved in acetone (100 mL) in a 500 mL three-necked bottle. Meanwhile, Fe_3O_4@OA nanoparticles were dispersed in n-hexane (100 mL) at a concentration of 4 mg/mL. The miscible liquids were heated up to 60°C and refluxed for 5 hours. A black precipitate (Fe_3O_4@DMSA nanoparticles) was obtained by magnetic separation and washed several times with double-distilled water. The Fe_3O_4@DMSA nanoparticles were dispersed in 50 mL double-distilled water by ultrasound. The solution was poured into a dialysis bag in water for 72 hours. The final sample (Fe_3O_4@DMSA) was filtrated with a 0.22 μm membrane. The phenanthroline method for determining the concentration of ferric ion in Fe_3O_4@DMSA nanoparticles has been detailed in the Supplementary materials (Figure S1A). The purified solution was stored at 4°C.

Synthesis of Fe_3O_4@DMSA@Ab magnetic nanoprobes

The nanoparticles of Fe_3O_4@DMSA were coupled with antibody via covalent bond formation between the free carboxylic groups of DMSA and the amine groups of rituximab. EDC (10 μg/μL, 10 μL) and sulfo-NHS (10 μg/μL, 5 μL) were added to 0.5 mL of Fe_3O_4@DMSA aqueous (1 mg) solution in borate buffer (0.04 M, pH 9) to activate the carboxylic groups. The activation reaction continued for 30 minutes in a thermostat oscillator at 25°C. Rituximab was then added to the mixture with further oscillation for 2 hours. The Fe_3O_4@DMSA@Ab nanoprobe solution was purified by gel chromatography (Sephacryl S-300 HR; GE Healthcare, Chicago, IL, USA) and the initial 1 mL from percolate of the Fe_3O_4@DMSA@Ab nanoprobes was collected. The remaining filtrates were carefully collected and tested to determine the rituximab content in the Fe_3O_4@DMSA@Ab sample (Figure S1B–D). After adding 110 μL aqueous BSA solution (10%), the Fe_3O_4@DMSA@Ab solution was stored at 4°C for follow-up experiments. The following percolates were collected to detect the amount of un-coupled antibodies using the BCA assay.

Characterization of nanoparticles and nanoprobes

The size and shape of Fe_3O_4@DMSA nanoparticles and Fe_3O_4@DMSA@Ab nanoprobes were characterized by transmission electron microscopy (TEM) using a JEM-2100 electron microscope (JEOL, Tokyo, Japan) with a working voltage of 200 kV. A drop of diluted particle solution in water was placed on a carbon-coated copper grid and dried overnight before observation. The sample of Fe_3O_4@DMSA@Ab was negatively stained with 2% sodium phosphotungstate (pH =7.0) to observe rituximab in the image.

The hydrodynamic size and zeta potential (ξ) values of Fe_3O_4@DMSA nanoparticles and Fe_3O_4@DMSA@Ab nanoprobes were measured using a dynamic light scattering device from Malvern Instruments (ZetaPlus; Brookhaven Instruments Corporation, Holtsville, NY, USA). The measured concentration was 0.1 mg [Fe]/mL. The saturation magnetization of Fe_3O_4@DMSA and Fe_3O_4@DMSA@Ab was determined using a vibrating sample magnetometer (VSM; LakeShore Cryotronics, Westerville, OH, USA) at room temperature in a field of up to 4 kOe.

Cell culture

Raji and K562 cells were purchased from the Type Culture Collection of the Chinese Academy of Sciences, Shanghai, China. FBS was heat-inactivated to eliminate the role of complement fixation in cell death by rituximab. Raji cells were cultured in RPMI-1640 medium containing 10% FBS and 1% penicillin-streptomycin at 37°C and 5% CO_2 in a humidified incubator. K562 cells were grown in IMDM culture medium supplemented with 10% FBS, 1% penicillin and streptomycin at 37°C and 5% CO_2 in a humidified incubator. Cells in the exponential phase were selected for further experiments.

Cell viability assay

Cytotoxicity of Fe_3O_4@DMSA nanoparticles and Fe_3O_4@DMSA@Ab nanoprobes was analyzed using a CCK-8 kit and Annexin V-FITC/PI double-staining assay. Raji cells and K562 cells were seeded in 96-well plates at a concentration of 2×10^4 cells/mL and treated with rituximab (0, 4.7, 9.4, 14.1, 18.8, 28.2, 37.6, and 47 μg/mL), Fe_3O_4@DMSA, and Fe_3O_4@DMSA@Ab (0, 10, 20, 30, 40, 60, 80, and 100 μg[Fe]/mL). After 24 hours (or 72 hours), 10 μL CCK-8 was added to each well and incubated at 37°C for 4 hours; absorbance was measured using a microplate reader (model 680; Bio-Rad Laboratories Inc., Hercules, CA, USA) at 450 nm. Raji and K562 cells treated with different concentrations of rituximab, Fe_3O_4@DMSA, and Fe_3O_4@DMSA@Ab were the experimental measurements (Read A) and the same concentration of Fe_3O_4@DMSA and Fe_3O_4@DMSA@Ab with culture medium alone was used as condition controls (Read B). The negative control was untreated cells (Read C). The blank control was medium exclusively (Read D). Cell viability was determined as follows: cell viability (%) = (A–B)/(C–D) × 100%.

Raji and K562 cells were cultured in six-well plates with rituximab (23.5 μg/mL), Fe_3O_4@DMSA, and Fe_3O_4@DMSA@Ab (50 μg[Fe]/mL) for 24 hours (or 72 hours). Next, Annexin V-FITC/PI staining was performed according to the manufacturer's recommended conditions. Briefly, the cell suspension was incubated with 5 μL Annexin V-FITC and 5 μL PI for 15 minutes at 37°C, away from light. Apoptotic and necrotic cells were analyzed on a flow cytometer (Calibur; BD Biosciences, San Jose, CA, USA).

Live/dead cell staining

The treated Raji and K562 cells were also stained with AO and EB. After treatment with rituximab (23.5 μg/mL), Fe_3O_4@DMSA, and Fe_3O_4@DMSA@Ab (50 μg[Fe]/mL) for 24 hours, the cells were centrifuged at 2,000 rpm for 5 minutes to remove the nanoparticles and nanoprobes, and the resuspended cells were incubated with a mixture of AO and EB for 30 minutes at 37°C without light and examined under a fluorescence microscope.

Location of Fe_3O_4@DMSA@Ab nanoprobes in cells

Raji and K562 cells were cultured in six-well cell culture plates with Fe_3O_4@DMSA and Fe_3O_4@DMSA@Ab (50 μg[Fe]/mL). Fe_3O_4@DMSA and Fe_3O_4@DMSA@Ab were removed by magnetic separation and centrifugation after 24 hours. The cells were then resuspended in PBS and fixed on glass slides by centrifugation. The nanoparticles were then stained blue with Pearls' dye and the cells were stained red with neutral red.

To determine whether the aggregation of Fe_3O_4@DMSA and Fe_3O_4@DMSA@Ab after co-incubation with cells over time can be detected by clinical MRI, the cell samples were prepared as follows: Raji and K562 cells were cultured in a six-well plate cell culture dish with different concentrations of Fe_3O_4@DMSA and Fe_3O_4@DMSA@Ab (0, 5, 10, 20, 50, and 100 μg[Fe]/mL). After a period of 24 hours, Fe_3O_4@DMSA and Fe_3O_4@DMSA@Ab centrifuged for three times to get rid of the suspended nanoparticles and nanoprobes. Cells were resuspended in a mixture of fresh culture medium and agarose gel in special glass bottles (bottles with no magnetic effects) before detection. MR images were obtained using a 1.5T MR scanner (Avanto; Siemens, Munich, Germany) with a head and neck coil. The T2 relaxation times were measured by turbo spin echo. The sequence parameters were as follows: repetition time (TR) =2,500 ms, echo time (TE) began at 22 ms and ended at 352 ms with the gap of 22 ms, matrix size 256×256, field of view FOV =3.5×3.5 cm, slice thickness =1 mm. Cell samples labeled with different concentration of Fe_3O_4@DMSA and Fe_3O_4@DMSA@Ab were observed. The T2 values were obtained by inverting the captured images and measuring within a region of interest of 0.25 cm^2.

In vitro TEM imaging of cells cultured with Fe_3O_4@DMSA@Ab nanoprobes

The ultrastructure of cells was also observed by TEM (JEM-2000EX; JEOL) after culturing with Fe_3O_4@DMSA@Ab nanoprobes. For control experiments, medium without nanoparticles was used. As above, the cells were washed and collected after co-culture. The cell clusters were then fixed with 2.5% glutaraldehyde for 24 hours and then treated with 1% osmium tetroxide for 1.5 hours. The cell clusters were dehydrated through ethanol at a series of different concentrations (20%, 30%, 40%, 50%, 60%, 70%, 90%, and 100%). The cell clusters were then soaked in propylene oxide (twice for 15 minutes each) and a mixture of propylene oxide and araldite resin overnight. Finally, the cell clusters were infiltrated with fresh araldite resin (three times, 3–4 hours each) followed by embedding in araldite resin at 60°C for 48 hours. The prepared cell clusters were cut into ultrathin sections with an ultramicrotome, stained with 1% uranyl acetate and 0.2% lead citrate, and then observed under TEM and photographed.

Intracellular calcium investigation

Raji and K562 cells were collected and suspended at a density of 10^7 cells/mL in Hank's Balanced Salt Solution (HBSS) after incubation with rituximab (23.5 μg/mL), Fe_3O_4@DMSA, and Fe_3O_4@DMSA@Ab (50 μg[Fe]/mL) for 24 hours. The cells were washed twice with HBSS and loaded with 5 μM of the calcium fluorescence indicator Fluo3-AM in HBSS buffer containing 0.04% (W/V) Pluronic F-127 at 37°C for 30 hours. Cells were then washed and suspended in HBSS buffer and fluorescence was read immediately on a flow cytometer.

Reactive oxygen species (ROS) generation

Intracellular generation of ROS was measured after Raji and K562 cells were exposed to rituximab (23.5 μg/mL), Fe_3O_4@DMSA, and Fe_3O_4@DMSA@Ab (50 μg [Fe]/mL) for 24 hours. Cells were then collected and loaded with 4 μL MDCFH-DA fluorescent marker in PBS for 20 minutes and then resuspended in PBS after washing with PBS (three times). Each sample was divided equally into two portions. The fluorescence of the first portion was recorded without light using the multi-scan Spectrum (Infinite M200; TECAN, Männedorf, Switzerland), at 488 nm excitation and 525 nm emission. The cell viability of the other portion was tested using the CCK-8 kit. For each sample, the ratio of fluorescence intensity and cell viability was measured to determine the intracellular production of ROS.

Detection of mitochondrial membrane potential (MMP) change

MMP was investigated using the fluorescent lipophilic cationic dye JC-1. Briefly, Raji and K562 cells were collected after treatment with rituximab (23.5 μg/mL), Fe_3O_4@DMSA, and Fe_3O_4@DMSA@Ab (50 μg[Fe]/mL) for 24 hours (or 72 hours). Cell clusters were then incubated with JC-1 at 37°C for 20 minutes. The fluorescence intensity of cell samples was assayed after washing with RPMI-1640 (three times) using flow cytometry (CaliburTM; BD Biosciences).

Western blot analyses

Following treatment, the cell lysates of all samples were collected and analyzed by western blotting to detect the levels of Bcl-2 and Bax proteins. The concentration of the cell lysate was measured using a protein assay kit. The primary antibodies against Bcl-2 and Bax were used in this study. The secondary antibody was horseradish peroxidase conjugated anti-rabbit IgG. All samples were separated on SDS-PAGE gels and transferred electrophoretically to polyvinylidene difluoride membranes according to standard procedures. After blocking with tris-buffered saline containing 0.1% Tween® 20 and 5% non-fat milk at room temperature for 2 hours, the membrane was incubated overnight with the primary antibody (1:1,000) at 4°C. After washing and subsequent blocking, the membrane was incubated with peroxidase conjugated secondary antibody (1:500) for 2 hours at room temperature, and subsequently stained with diaminobenzidine. Anti-β-actin was used as a control to ensure equal loading. Detection was performed using an enhanced chemiluminescence kit and an ECL system.

Raji cell apoptosis under a MF

Raji cells were incubated with Fe_3O_4@DMSA and Fe_3O_4@DMSA@Ab (50 μg [Fe]/mL) for 12 hours without MF (mean field strength 1,547.2±146.7 Gs, measured by numerical type BST600 Gauss Meter (Hangzhou Perfect Technology Co., Ltd., Hangzhou, China). The cells were then harvested and divided equally into two portions. One portion was resuspended in fresh culture medium for another 12 hours under MF. The other portion was cultured in fresh RPMI-1640 for 12 hours without MF in the subsequent steps. Together with untreated cells, cells treated with MF were harvested and subjected to flow cytometry (CaliburTM; BD Biosciences) analysis.

Statistical analysis

Statistical analysis was performed using Graph pad 5.0 and Origin 8.0 software packages. Measurements of each treatment were repeated at least three times. The data obtained are presented as mean ± standard deviation (SD). Statistical comparisons were computed using two- or three-way ANOVA or an unpaired *t*-test. The data were considered significant at P-values<0.05 (*) or highly significant at $P<0.01$ (**).

Results and discussion

Synthesis and characterization of Fe_3O_4@DMSA@Ab nanoprobes

Among all the methods to synthesize Fe_3O_4 nanoparticles, co-precipitation is the classical and most efficient chemical pathway.[33] In this paper, co-precipitation was used to prepare OA modified Fe_3O_4 nanoparticles. The Fe_3O_4@OA nanoparticles were dispersed in n-hexane for their oil-solubility. However, they needed to be converted into the aqueous phase for further biological applications. Thus, DMSA was chosen to exchange OA on the surface of the nanoparticles. DMSA

is a non-toxic agent that can be used for treating plumbism.[34] Its metal chelating agent, which forms strong complexes with Fe_3O_4 nanoparticles, allowed us to obtain a stable colloid in water, as indicated by monitoring hydrodynamic size variation for 35 days (Figure S2A). DMSA was found to form polydisulfide species $(DMSAox)_4$ on the surface of nanoparticles.[35] Furthermore, part of the –COOH groups remained free, which could be used for coupling antibodies.[36]

The process of synthesis of nanoparticles and nanoprobes is shown in Figure 1A. TEM results show that the Fe_3O_4@

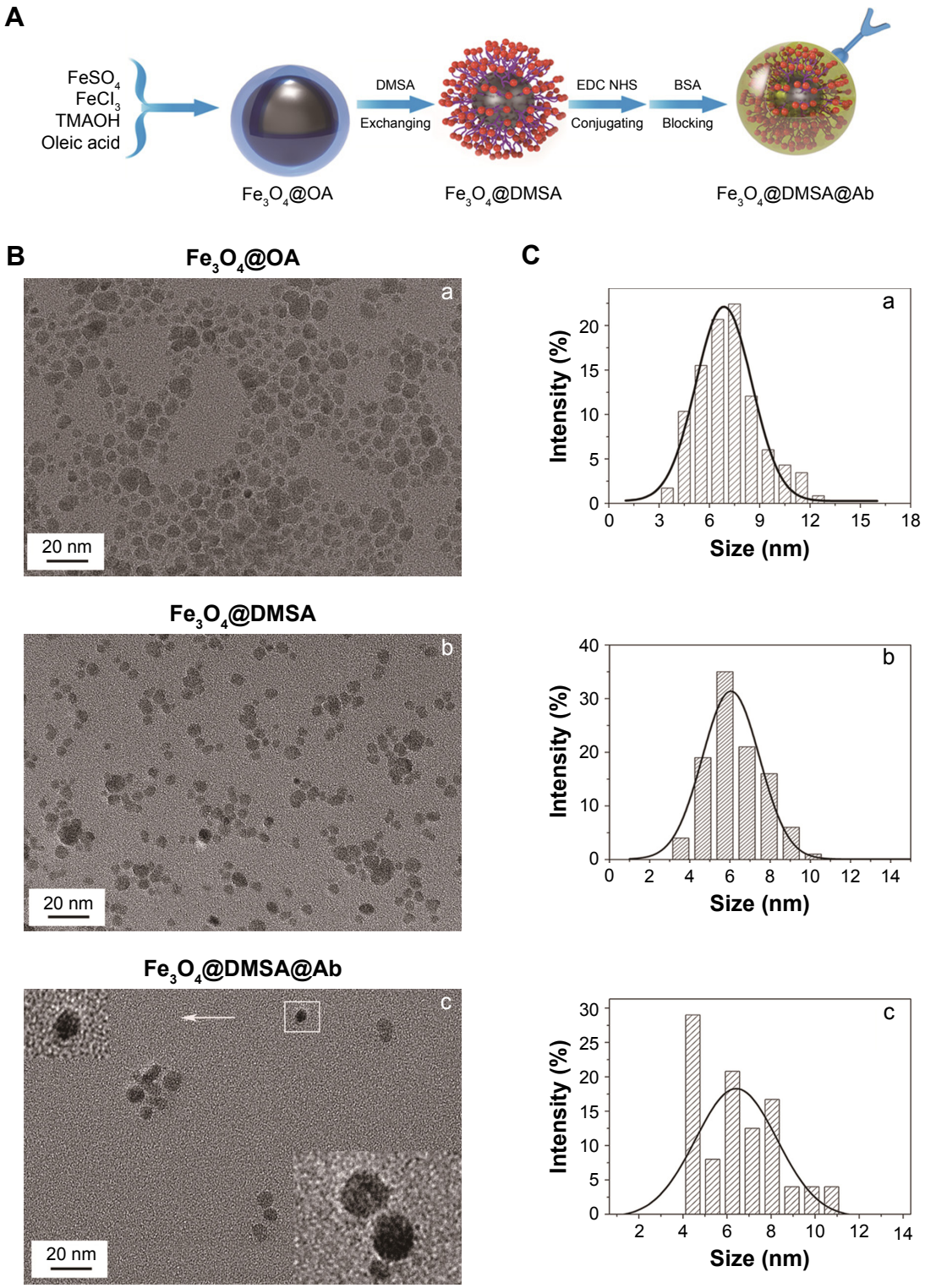

Figure 1 (*Continued*)

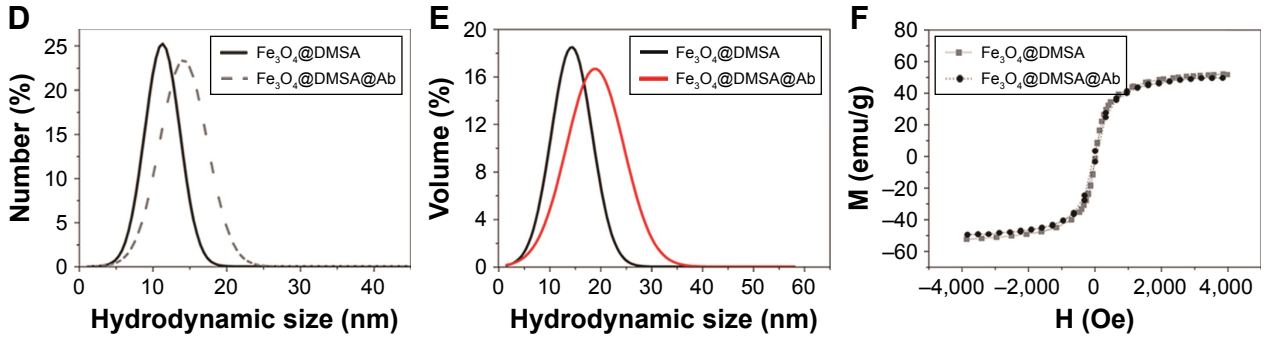

Figure 1 Schematic representation of the Fe_3O_4@OA, Fe_3O_4@DMSA nanoparticles and Fe_3O_4@DMSA@Ab nanoprobes (**A**). Representative TEM imaging (**B**) and core diameter (**C**) analysis of the Fe_3O_4@OA (**B**(a), **C**(a)), Fe_3O_4@DMSA (**B**(b), **C**(b)) nanoparticles and Fe_3O_4@DMSA@Ab (**B**(c), **C**(c)) nanoprobes. Hydrodynamic size in number (**D**) and in volume (**E**) analysis of the Fe_3O_4@DMSA nanoparticles and Fe_3O_4@DMSA@Ab nanoprobes dispersed in water and stored at 4°C. The saturation magnetization (**F**) of the Fe_3O_4@DMSA nanoparticles and Fe_3O_4@DMSA@Ab nanoprobes.
Abbreviations: DMSA, 2,3-dimercaptosuccinic acid; TEM, transmission electron microscopy; TMAOH, tetramethylammonium hydroxide.

DMSA nanoparticles are nearly spherical with an average diameter of 6.5±1.4 nm (Figure 1B(b) and C(b)), which is a little smaller than that of Fe_3O_4@OA nanoparticles (7.5±2.5 nm) (Figure 1B(a) and C(a)). The reason for these differences lies in the separation and washing during the post-processing part of the substitution reaction. Negative staining TEM was also performed to observe the rituximab layer coupled on the surface of Fe_3O_4@DMSA nanoparticles (Figure 1B(c) and C(c)).

The mean hydrodynamic size in number of the Fe_3O_4@DMSA nanoparticles was 11.3±2.4 nm (poly-dispersion index [PDI] <0.03) whereas that of the Fe_3O_4@DMSA@Ab was 14.1±3.2 nm (PDI <0.05) (Figure 1D). The mean hydrodynamic size in volume of Fe_3O_4@DMSA nanoparticles was 14.3±4.0 nm (PDI <0.03) whereas that of the Fe_3O_4@DMSA@Ab was 18.9±5.6 nm (PDI <0.05) (Figure 1E). Fe_3O_4@DMSA carries a negative zeta potential of −40.6 mV whereas the zeta potential of Fe_3O_4@DMSA@Ab nanoprobes is −37.0 mV (Figure S2E). These results indicate the presence of rituximab on the surface of Fe_3O_4@DMSA nanoparticles.[37] The obtained Fe_3O_4@DMSA@Ab was stable in aqueous solution as evaluated by monitoring the variation in hydrodynamic size during storage at 4°C within a month (Figure S2B). The stability of Fe_3O_4@DMSA nanoparticles and Fe_3O_4@DMSA@Ab nanoprobes in RPMI-1640 cell culture medium was carefully measured by monitoring their hydrodynamic size variation (Figure S2C and D). The Fe_3O_4@DMSA exhibited large hydrodynamic size which originated from nanoparticle aggregation and thus poor colloidal stability in RPMI-1640, due to the lack of steric stabilizations. By comparison, Fe_3O_4@DMSA@Ab displayed smaller hydrodynamic size, but a state of aggregation, due to antibody conjugation and BSA blocking on the surface of nanoparticles.

The hysteresis loops of Fe_3O_4@DMSA and Fe_3O_4@DMSA@Ab are shown in Figure 1F. The saturated magnetization for Fe_3O_4@DMSA and Fe_3O_4@DMSA@Ab is 51.7 emu/g [Fe] and 49.7 emu/g [Fe], respectively, it was demonstrated that the sample is a superparamagnetic from the hysteresis loop.

Rituximab antibodies were conjugated on the surface of Fe_3O_4@DMSA nanoparticles by EDC/NHS to obtain stable Fe_3O_4@DMSA@Ab nanoprobes. To further quantify the conjugated antibody, the elemental Fe and antibody levels were determined using phenanthroline method and a BCA kit. The results indicated that the final Fe_3O_4@DMSA@Ab nanoprobe solution contained 5 μg of Fe and 2.35 μg of antibodies per 10 μL. The average numbers of antibodies conjugated on each nanoparticle can be calculated according to the following equation:

$$M_{Fe_3O_4} = \frac{4}{3}\pi\left(\frac{D}{2}\right)^3 \rho_{Fe_3O_4} = 7.44\times10^{-19}\,g \quad (1)$$

$$N_{Fe_3O_4} = \frac{m_{Fe_3O_4}}{M_{Fe_3O_4}} = 9.25\times10^{12} \quad (2)$$

$$M_{rituximab} = 150\ KDa \quad (3)$$

$$N_{rituximab} = \frac{m_{rituximab}}{M_{rituximab}} \times N_A = 9.43\times10^{12} \quad (4)$$

$$R_{Rituximab/Fe_3O_4} = \frac{N_{rituximab}}{N_{Fe_3O_4}} = 1.01 \quad (5)$$

where $M_{Fe_3O_4}$ is the mass of a single Fe_3O_4 nanoparticle and $M_{rituximab}$ is the molecular weight of rituximab. $m_{Fe_3O_4}$ and $m_{rituximab}$ indicate the mass of Fe_3O_4 nanoparticles and rituximab antibody in 10 μL solution, respectively. $N_{Fe_3O_4}$ and $N_{rituximab}$ indicate the number of Fe_3O_4 nanoparticles and rituximab molecules, respectively. D is the average diameter

of Fe_3O_4@DMSA nanoparticles, and $\rho_{Fe_3O_4}$ is the density of Fe_3O_4. It is obvious that $R_{Rituximab/Fe_3O_4}$ represents the number of rituximab molecules conjugated on the surface of one Fe_3O_4 nanoparticle, which is about 1.

Fe_3O_4@DMSA@Ab nanoprobe specifically targets CD20

It is well known that expression of the integral membrane protein CD20 is found on pre-, naïve, and mature B cells in malignancies but not on plasma cells or early pro-B cells.[38] CD20 is an ideal target for rituximab therapy because of its presence in the majority of B-cell lymphomas.[39] The process of Fe_3O_4@DMSA@Ab nanoprobe targeting and staining is shown in Figure 2A. CD20 expression on Raji cells was detected using a T/B cell lymphoma immunohistochemical double-dye diagnostic kit (Figure 2B[b]).

The rituximab immobilized on the surface of Fe_3O_4@DMSA nanoparticles was captured by CD20 on the Raji cell

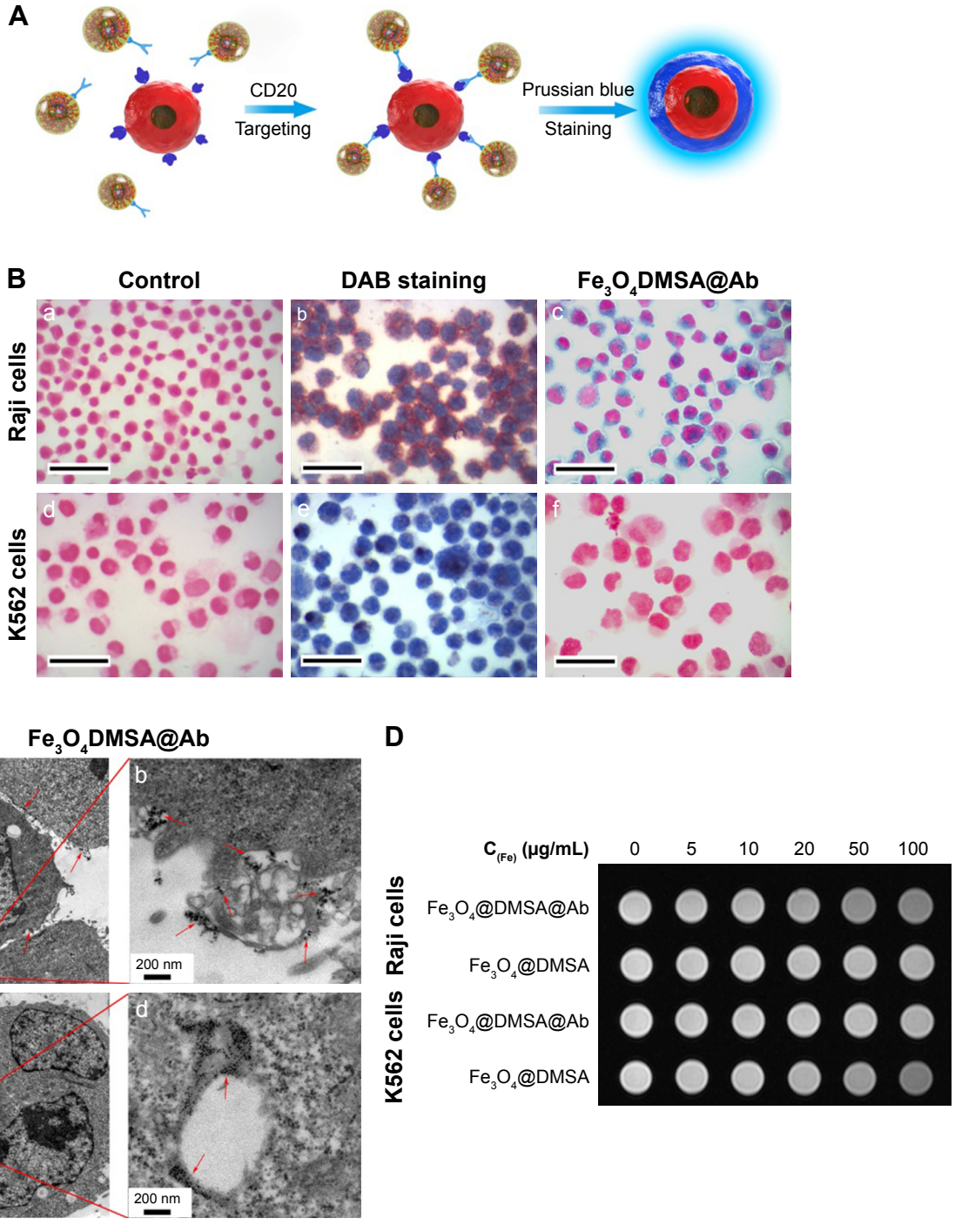

Figure 2 (*Continued*)

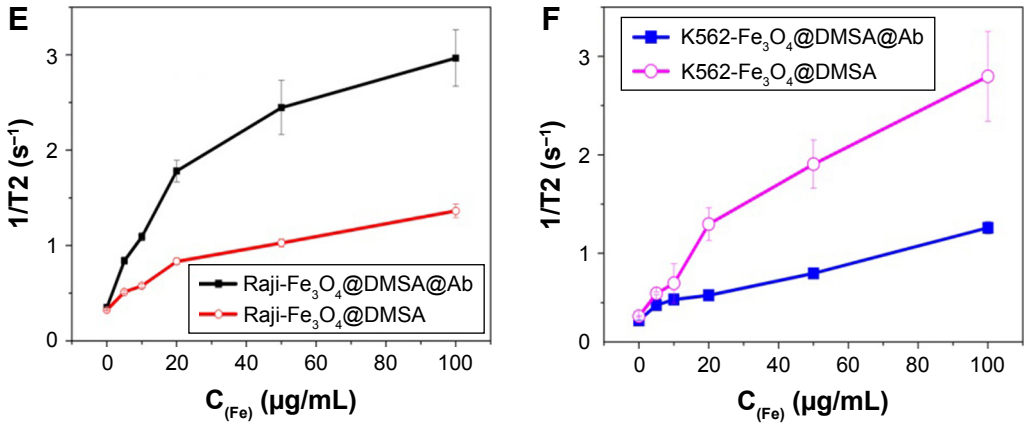

Figure 2 Schematic representation of Raji cells labeling with Fe_3O_4@DMSA@Ab nanoprobes and staining with Prussian blue for Fe (**A**). Detection of CD20 on the surface of Raji cells with a T/B kit and Fe_3O_4@DMSA@Ab (**B**, scale bar 100 μm). Control groups of Raji cells (**B**(a)) and K562 cells (**B**(d)). Detection of CD20 on Raji cells (**B**(b)). CD3 detecting on K562 cells (**B**(e)). Fe_3O_4@DMSA@Ab-labeled Raji cells (**B**(c)) and K562 cells (**B**(f)). TEM images of Raji (**C**(a, b)) and K562 (**C**(c, d)) cells incubated with Fe_3O_4@DMSA@Ab. MRI detection of Fe_3O_4@DMSA and Fe_3O_4@DMSA@Ab-labeled Raji cells (**E**) and K562 cells (**F**) and the corresponding 1/T2 variation as a function of [Fe] concentration (**D**).
Abbreviations: DMSA, 2,3-dimercaptosuccinic acid; TEM, transmission electron microscopy.

membrane. Fe_3O_4@DMSA nanoparticles without rituximab cannot be recognized by Raji cells. With the addition of Prussian blue staining buffer,[27,40] iron was dyed blue. The targeting effect of Fe_3O_4@DMSA@Ab nanoprobes was determined in both living cells and immobilized cells. In living cells, Fe_3O_4@DMSA@Ab nanoprobes were located on the surface of Raji cells, conferring their ability to target CD20 (Figure S3). This is consistent with previous studies where CD20 is not internalized after antibody binding.[41,42] Fe_3O_4@DMSA nanoparticles were located neither in the cytoplasm nor in the cytomembrane of Raji cells.

K562 cells were found to phagocytize Fe_3O_4@DMSA nanoparticles. The lighter blue indicates that the uptake of Fe_3O_4@DMSA@Ab nanoprobes by K562 cells was less than the uptake of Fe_3O_4@DMSA nanoparticles. This is likely because the nanoprobes were unrecognizable to the K562 cells, and the antibody conjugation and BSA blocking reduced the non-specific adsorption of nanoparticles. This result is also verified by TEM analysis (Figure 2C(a and b)). To exclude the uptake effect of living cells, Raji and K562 cells were collected and fixed on slides with paraformaldehyde after centrifugation. The blue around the Raji cells indicates that the nanoprobes were labeled on the cell surface (Figure 2B(c)). There is no blue staining in K562 cells due to the absence of CD20 protein (Figure 2B(f)).

Imaging of Fe_3O_4@DMSA or Fe_3O_4@DMSA@Ab-labeled Raji cells and K562 cells was also performed on a clinical magnetic resonance scanner (MRI). The relaxation rate (1/T2) values of cell phantoms changed with increasing Fe concentration (Figure 2D). Raji cells incubated with Fe_3O_4@DMSA@Ab had the highest relaxation rate for specific binding and subsequent aggregation of nanoparticles on the cell surface after co-incubation.[43,44] With increasing nanoprobe dosages, they were more bound onto Raji cell membrane, leading to stronger MR signal. This result is consistent with the Prussian blue staining (Figure S3). Meanwhile, the nanoprobe aggregation on the surface of cell membrane also contributed to the enhanced MR signal. The aggregations of Fe_3O_4@DMSA@Ab could be confirmed from the TEM results of treated cells (Figure 2C). By comparison, Fe_3O_4@DMSA nanoparticles show little enhancement in relaxation rate on Raji cells with increasing concentrations (Figure 2D–F).

The relaxation rate of K562 cells incubated with Fe_3O_4@DMSA nanoparticles is higher than that of Raji cells. This result is mainly due to more active endocytosis in K562 cells and gradual intracellular accumulation in lysosome (Figure 2C) with increasing dosages of Fe_3O_4@DMSA nanoparticles. The cellular uptake of Fe_3O_4@DMSA@Ab nanoprobes in K562 cells may be inhibited by conjugating the rituximab antibody and BSA blocking, which is consistent with the results of Prussian blue staining (Figure S3).

Fe_3O_4@DMSA@Ab nanoprobes induce apoptosis in a concentration- and time-dependent manner

CCK-8 assay was carried out to evaluate the cytotoxicity of rituximab, Fe_3O_4@DMSA, and Fe_3O_4@DMSA@Ab in Raji and K562 cells. BB buffer without nanoparticles and nanoprobes did not reduce Raji and K562 cell viability (Figure S4). The viability of Raji cells treated with Fe_3O_4@DMSA@Ab nanoprobes was reduced to 70% even at a concentration of 20 μg[Fe]/mL, and was further decreased with increasing iron concentration. Compared with rituximab

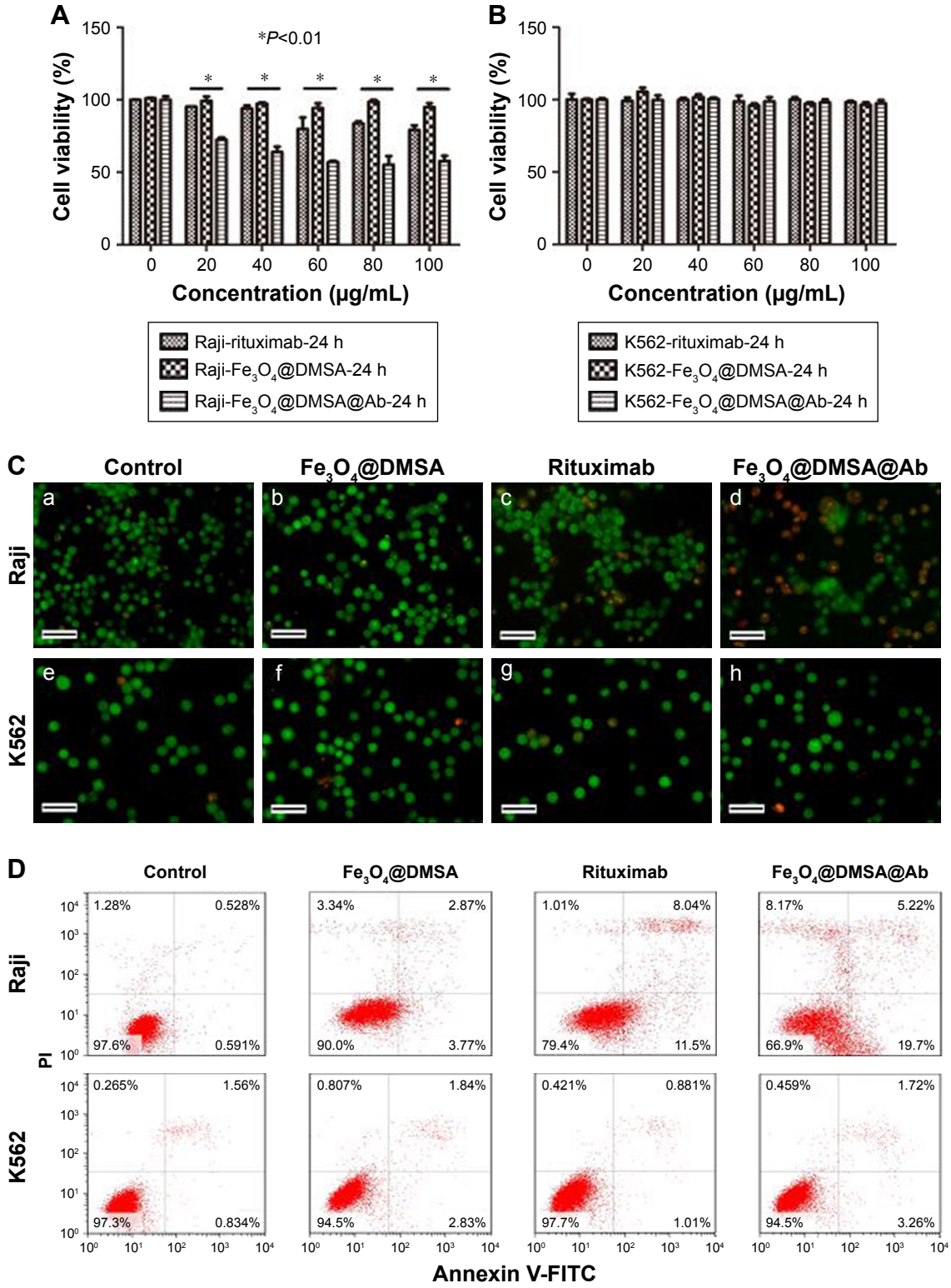

Figure 3 Viability and apoptosis of Raji and K562 cells after culturing with rituximab, Fe_3O_4@DMSA, and Fe_3O_4@DMSA@Ab for 24 hours, detected by CCK-8 (**A**, **B**), AO/EB fluorescence staining (**C**, Scale bar 100 μm), and FlowCytometry (**D**) of Raji and K562 cells after 24 h.
Abbreviations: DMSA, 2,3-dimercaptosuccinic acid; CCK-8, cell counting kit-8.

alone,[45] Fe_3O_4@DMSA@Ab displayed stronger cytotoxicity to Raji cells, and there was a statistically significant difference between the rituximab and Fe_3O_4@DMSA@Ab groups ($P<0.05$) in 24 hours (Figure 3A) and 72 hours (Figure S5A). The Fe_3O_4@DMSA nanoparticles did not notably alter the Raji cell viability at various concentrations (Raji cell viability >90%). These results (Figures 3 and S5) revealed that none of the agents had a significant influence on K562

cell viability at the corresponding concentration range after culturing for 24 and 72 hours (K562 cell viability >90%).

Fe_3O_4@DMSA@Ab-mediated Raji cell apoptosis was further observed by AO and EB double staining of cell nuclei,[46] and rituximab and Fe_3O_4@DMSA used for comparison. Fluorescence microscopy images of the dual stained Raji and K562 cells are presented in Figure 3C. The results show that live Raji cells were stained green due to AO uptake and their numbers decreased upon treatment with rituximab or Fe_3O_4@DMSA@Ab, which is consistent with the CCK-8 data. It can be observed that there is an obvious increase of orange cells in the Fe_3O_4@DMSA@Ab-treated Raji cell group for the uptake of EB, which can be attributed to cell membrane perforation during apoptosis. In K562 cells, there were no significant changes in green cell numbers for all four group, indicating the non-toxicity of nanoparticles and nanoprobes to K562 cells without CD20 expression (Figure 3C).

Apoptosis after treatment with rituximab, Fe_3O_4@DMSA nanoparticles, and Fe_3O_4@DMSA@Ab nanoprobes was detected using the Annexin V-FITC/PI assay with flow cytometry. The results show that rituximab, Fe_3O_4@DMSA, and Fe_3O_4@DMSA@Ab had no obvious effect on K562 cells with increasing time and dose for 24 hours (Figure 3D) and 72 hours (Figure S5C). The results also indicated that both rituximab and Fe_3O_4@DMSA@Ab nanoprobes could lead to Raji cell death in a time-dependent manner. The total quantity of early apoptotic Raji cells in the Fe_3O_4@DMSA@Ab group (19.7%) is higher than the sum of that in the rituximab and Fe_3O_4@DMSA groups (15.27%, 3.77% plus 11.5%). Though the late apoptotic Raji cells in the Fe_3O_4@DMSA@Ab group (5.22%) are less than those in the rituximab group (8.22%), the cellular debris in the Fe_3O_4@DMSA@Ab group (8.17%) is greater than that in the rituximab (1.10%) and Fe_3O_4@DMSA (3.34%) groups. In addition, the Raji cells show lower levels of viability upon treatment with Fe_3O_4@DMSA@Ab (66.9%) compared to treatment with rituximab (79.4%) or Fe_3O_4@DMSA (90.0%) only. This suggests that the mechanism of the Fe_3O_4@DMSA@Ab inhibitory effect seems to include apoptosis induction as well as generation of cell fragments, which results in a synergistic effect of the nanoparticle-antibody conjugates.

Fe_3O_4@DMSA@Ab nanoprobe triggers an increase in intracellular Ca^{2+}

As a second messenger, calcium plays an important role in signal transduction and the regulation of cell activity. Evidence has shown that calcium may be related to apoptosis.[47,48] Studies support the hypothesis that CD20 is a central component of the calcium ion channel.[39] The transmembrane structure and homotypic aggregation of CD20 itself after cross-linking with antibodies forms an ion channel.[39,49] Intracellular Ca^{2+} concentration is known to be related to CD20 expression level while the cell is in a resting state.[50,51] Perturbation of Ca^{2+} homeostasis triggers apoptosis following the binding of CD20 with rituximab.[16] We hypothesized that the possible mechanism of pro-apoptosis is related to Ca^{2+}, ROS, and $\Delta\Psi m$ (Figure 4A). For this, intracellular calcium was detected using Fluo 3-AM in Raji cells, and intracellular calcium is increased after culturing with Fe_3O_4@DMSA@Ab for 24 hours (Figure 4C) or 72 hours (Figure S6A) compared to the control, rituximab, and Fe_3O_4@DMSA groups. In comparison, none of the tested groups showed perturbation of Ca^{2+} in K562 cells after 24 hours (Figure 4C) or 72 hours (Figure S6B) in the absence of CD20. Ca^{2+} is reported to play an important role in apoptosis induction. Apoptosis induced by Fe_3O_4@DMSA together with rituximab in a physical mixture is lower than that in the Fe_3O_4@DMSA@Ab group. These results demonstrate that apoptosis induced by Fe_3O_4@DMSA@Ab requires CD20 cross-linking with the nanoprobes and they function in response to the increase in intracellular Ca^{2+}.

Fe_3O_4@DMSA@Ab nanoprobes trigger ROS generation and mitochondrial depolarization

ROS consist of oxidation molecules, ions, and free radicals. They exist widely in the human body and play important roles in most physiological and pathological processes. Intracellular ROS at high concentrations typically lead to a cytotoxic event.[52] Raji cells exposed to Fe_3O_4@DMSA@Ab nanoprobes show a significant ($P<0.001$) increase in ROS generation after 24 hours (Figure 4D) and 72 hours (Figure S6C). Moreover, ROS generation in the Fe_3O_4@DMSA@Ab nanoprobe group was two times greater than that in the rituximab group, resulting in stronger cytotoxicity. Notably, Fe_3O_4@DMSA nanoparticles also increase the levels of ROS in Raji cells, but no significant influence is observed in K562 cells, likely due to differences in their oxidative stress reactions with Fe_3O_4@DMSA nanoparticles.[53] The ROS level in each group showed no obvious changes on K562 cells after culturing for 24 hours (Figure 4D) and 72 hours (Figure S6C).

The apoptosis of Raji cells under the physical mixture of rituximab and Fe_3O_4@DMSA nanoparticles was tested to evaluate the effect of Fe_3O_4@DMSA@Ab nanoprobe. As shown in Figure 4E, Raji cell apoptosis was not markedly increased in the physical mixture of rituximab and Fe_3O_4@DMSA nanoparticles group than in the free rituximab group, which was also much lower than that in the Fe_3O_4@DMSA@Ab nanoprobe group.

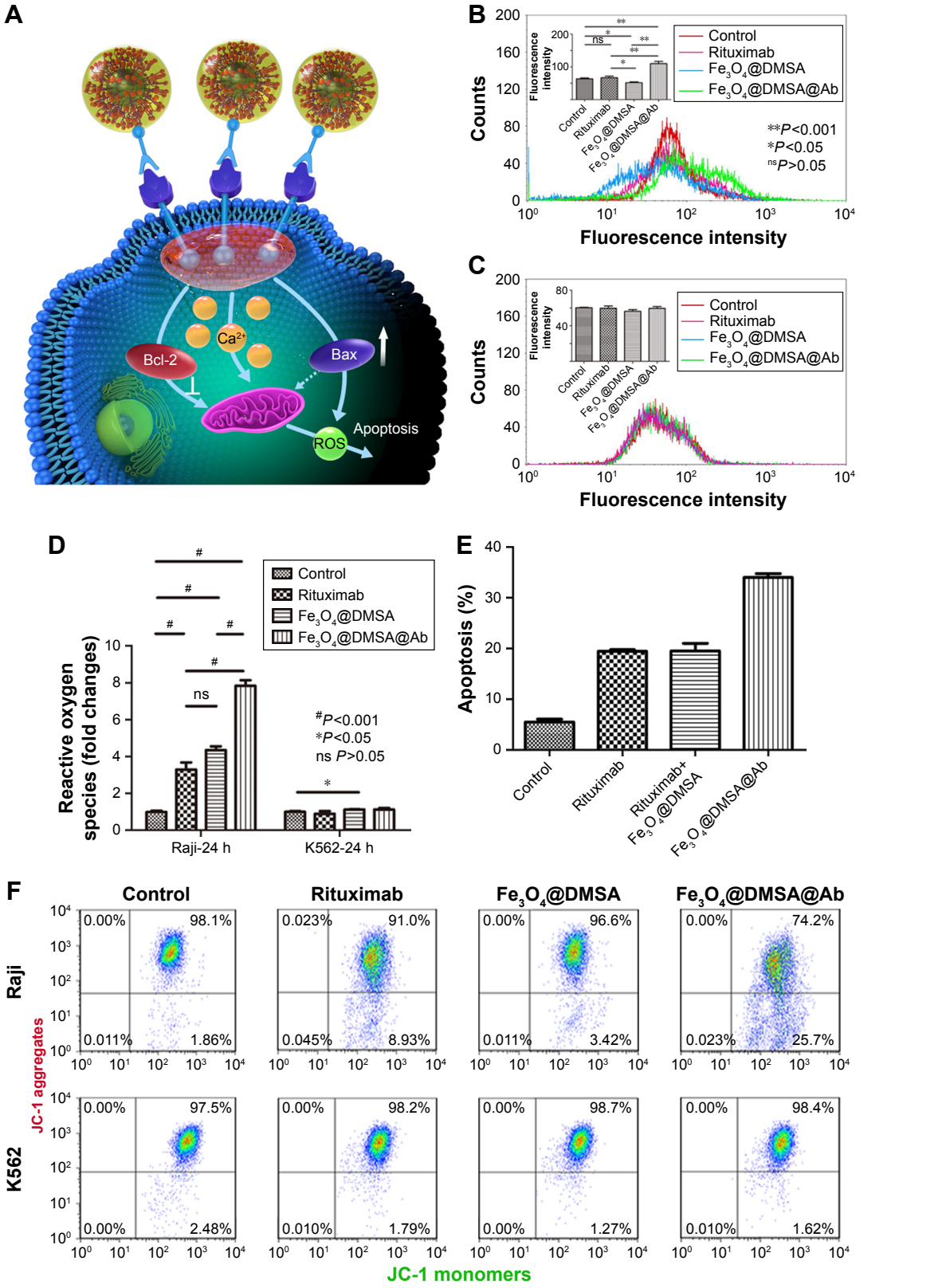

Figure 4 Schematic illustration of the possible mechanism of Fe_3O_4@DMSA@Ab-mediated apoptosis in Raji cells (**A**). The intracellular Ca^{2+} flux of Raji cells (**B**) and K562 cells (**C**) after incubation with rituximab, Fe_3O_4@DMSA, and Fe_3O_4@DMSA@Ab for 24 hours. Measurement of corresponding intracellular ROS (**D**) and mitochondrial membrane potential ($\Delta\Psi m$) (**F**) in cells. Apoptosis evaluation of Raji cells after incubating with or without rituximab, rituximab and Fe_3O_4@DMSA together, and Fe_3O_4@DMSA@Ab (**E**).

Abbreviation: DMSA, 2,3-dimercaptosuccinic acid.

ROS, Ca^{2+}, Bax, and other triggers could mediate the opening of mitochondrial permeability transition pores (MPTP),[53] inducing dissipation of ΔΨm and rupture of the mitochondrial outer membrane to release proteins.[54] The mitochondrial damage in turn leads to uncontrolled ROS formation. ΔΨm can be detected by the fluorescent JC-1 assay.[55] JC-1 can easily enter the mitochondria in normal cells (driven by ΔΨm), where it aggregates, emitting red fluorescence. When the ΔΨm collapses, JC-1 diffuses from mitochondria to the cytoplasm where it exists as a green-fluorescent monomer. Disruption of ΔΨm is considered to signal the start of the apoptotic process.[54,56] The scatter plots in the right upper quadrant represent high ΔΨm (Figure 4F control group). Upon loss of red fluorescence, the scatter plots are shifted to the right lower quadrant indicating a decrease in ΔΨm.

It is observed that Fe_3O_4@DMSA@Ab induces a more obvious drop of ΔΨm in Raji cells compared to the rituximab and Fe_3O_4@DMSA groups, which was clearly detected after incubation for 24 hours (Figure 4F) and 72 hours (Figure S6D). In contrast, K562 cells used as a negative control did not suffer any changes in their ΔΨm when exposed to similar treatments, indicating that there was no mitochondrial damage and that the K562 cells remained vital after incubation for 24 hours (Figure 4F) and 72 hours (Figure S6D).

Fe_3O_4@DMSA@Ab nanoprobes reduce the expression of Bcl-2 protein after treatment

The presence of Bcl-2 family proteins in the mitochondrial membrane has a functional connection.[57] Bcl-2 can protect the cell from apoptosis by preventing mitochondrial disruption.[54,57] Bax, a pro-apoptotic protein targets the mitochondrial membrane and can induce mitochondrial membrane damage and cell death without caspase activation.[58] Evidence suggests that Bax together with other proteins can form channels with a larger pore size in the outer mitochondrial membrane.[59,60] It is also reported that rituximab can inhibit the signaling pathways of p38 MAPK, NF-Kb, and Akt, which can inhibit the expression of Bcl-2.[61–63] Therefore, it is interesting to investigate the change in Bax/Bcl-2 upon treatment with Fe_3O_4@DMSA@Ab, thereby reducing their positive influence on apoptosis. The expression of anti-apoptotic protein Bcl-2 in Raji cells treated with Fe_3O_4@DMSA@Ab was markedly reduced compared with other groups, however, the expression of pro-apoptosis protein Bax was increased (Figure 5), suggesting that the nanoprobes can induce apoptosis in Raji cells. Meanwhile, Bcl-2 and Bax are nearly unchanged among the four groups in K562 cells.

Fe_3O_4@DMSA@Ab nanoprobes enhanced Raji cell apoptosis under a MF

In resting cells, CD20 multimers (probably at least tetramers) are distributed in mini-lipid raft domains of the cytomembrane. Binding of the anti-CD20 antibody causes clustering of CD20 multimers and their transfer to large lipid rafts, resulting in a CD20-mediated signaling cascade.[39] These signals include activation of tyrosine protein kinase, influx of Ca^{2+}, and phospholipase Cγ2 (PLCγ2) phosphorylation.[11] CD20 cluster formation is also reported to increase with the addition of a secondary antibody, which acts as a bridge to

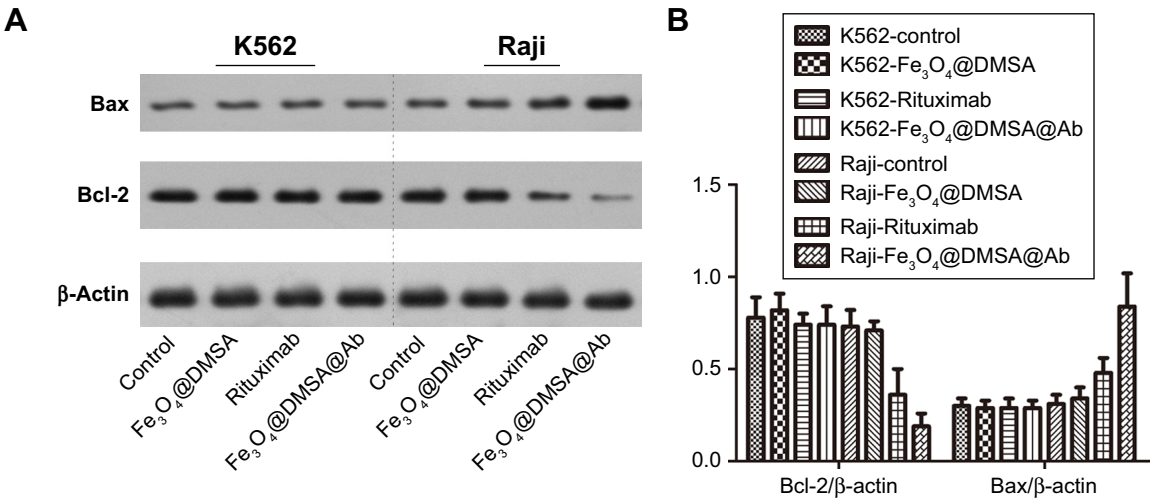

Figure 5 Expression of Bcl-2 and Bax protein after treatment of Raji and K562 cells with rituximab, Fe_3O_4@DMSA, and Fe_3O_4@DMSA@Ab (**A**), and the corresponding changes in Bcl-2/β-actin and Bax/β-actin (**B**).
Abbreviation: DMSA, 2,3-dimercaptosuccinic acid.

crosslink the CD20 antibodies. The secondary antibody was not added in our experiment, whereas Raji cell apoptosis was increased in the Fe_3O_4@DMSA@Ab group. The magnetic dipole interactions among these nanoprobes after binding with CD20, which led to form nanoprobe clusters and CD20 clusters, may be one of the important causes of apoptosis.[64] These nanoprobe clusters exhibit large magnetic dipole moments compared to a single nanoprobe, which is inclined to form larger aggregates. Conversely, when the contact distance of nanoprobes is too large, the weak magnetic dipole interactions between nanoprobes are not sufficient to result in cluster formation. We therefore investigated whether apoptosis in Raji cells treated with magnetic Fe_3O_4@DMSA@Ab nanoprobes increases upon exposure to a MF.

As per the schematic illustration in Figure 6A, Fe_3O_4@DMSA@Ab was incubated with Raji cells for 12 hours, and they were captured by CD20 on the cell membrane. Raji cells were collected after centrifugation to remove the free Fe_3O_4@DMSA@Ab and exposed to static MF for another 12 hours. Compared with Raji cells without MF exposure, Raji cells under static MF suffer increased apoptosis (Figure 6B). The morphological changes in Raji cells are shown in Figure S7. The percentage of viable non-apoptotic Raji cells varied from 73.8% without MF (Figure 6B) to 61.7% with MF (Figure 6B). Obviously, the viability of Raji cells with Fe_3O_4@DMSA@Ab under static MF (61.7%, Figure 6B) is less than that with Fe_3O_4@DMSA@Ab without static MF for 24 hours (68.6%, Figure 6B), comfirming the above hypothesis. Static MF induces the aggregation of Fe_3O_4@DMSA@Ab nanoprobes on the cell membrane and thus induces CD20 cluster formation, resulting in Raji cell apoptosis. The survival fraction of Fe_3O_4@DMSA-treated Raji cells does not change significantly without or with static MF (90.2% to 89.7%, Figure 6B).

Based on these results, we hypothesized the possible mechanism of pro-apoptosis induced by Fe_3O_4@DMSA@Ab nanoprobes (Figure 4A). The clusters of CD20 and Fe_3O_4@DMSA@Ab nanoprobes induced by the magnetic dipole lead to increased intracellular Ca^{2+} and subsequently induce depolarization of $\Delta\Psi m$, mitochondrial damage, and uncontrolled ROS formation, which cause irreversible cell apoptosis. Meanwhile, the downregulation of Bcl-2 and upregulation of Bax further promote the dissipation of $\Delta\Psi m$ and apoptosis generation. The magnetic dipole interaction and homotypic adhesion can be enhanced by MF leading to accelerated Raji cell apoptosis. A possible explanation is that driving

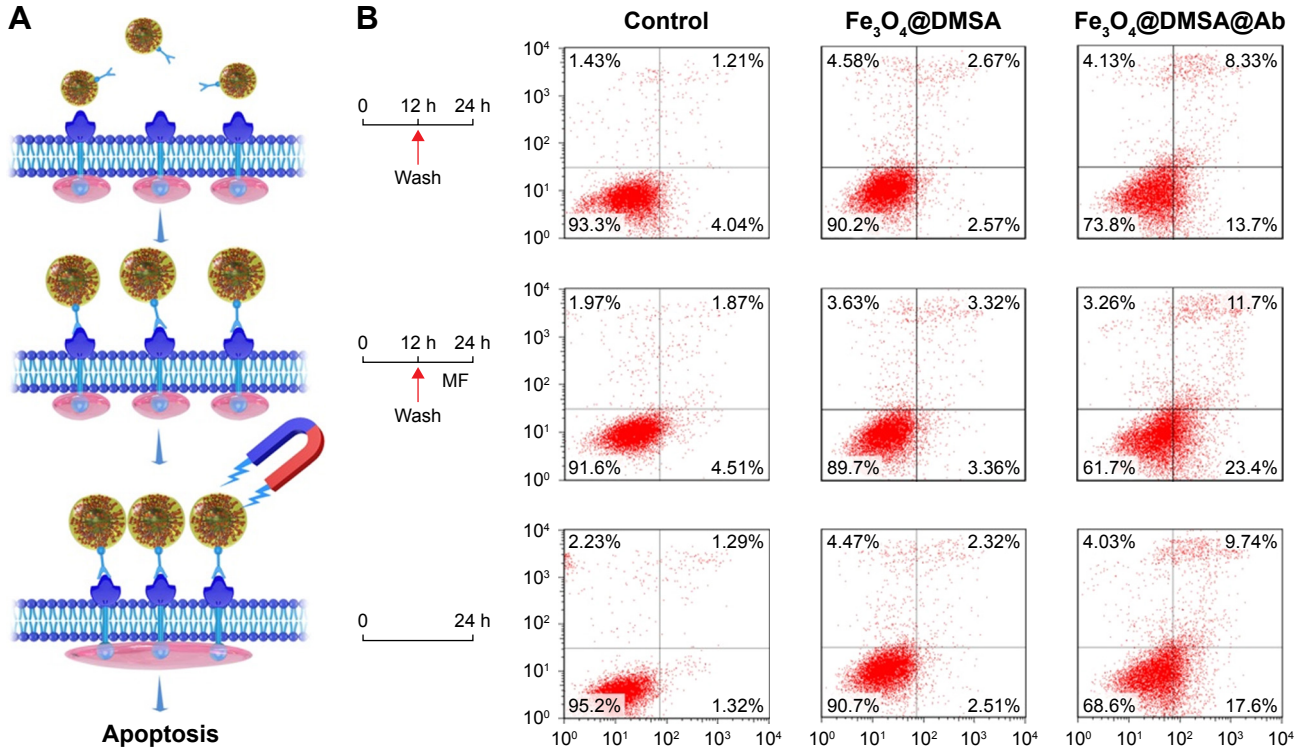

Figure 6 Schematic representation of CD20 clusters induced by Fe_3O_4@DMSA@Ab in the presence of a static magnetic field (**A**). Apoptosis of Raji cells detected by flow cytometry (**B**), Raji cells treated with Fe_3O_4@DMSA in the presence and absence of MF, Raji cells treated with Fe_3O_4@DMSA@Ab in the presence and absence of MF, and Raji cells treated with Fe_3O_4@DMSA@Ab for 24 hours.
Abbreviations: DMSA, 2,3-dimercaptosuccinic acid; FACS, FlowCytometry; MF, magnetostatic field.

by MF, Fe_3O_4@DMSA@Ab nanoprobes binding to CD20 (as a calcium ion channel on cell membranes), results in further disequilibrium of intracellular calcium homeostasis, playing an essential role in the process of rituximab-driven caspase-independent apoptosis.[16,65]

Conclusion

Magnetic nanoprobes of Fe_3O_4@DMSA@Ab were established to target the CD20 antigen and promote Raji cell apoptosis in vitro. These nanoprobes are composed of magnetic Fe_3O_4@DMSA nanoparticles and the commercial antibody rituximab. The Fe_3O_4@DMSA nanoparticles are nearly spherical and stable in aqueous solution. The number of rituximab molecules conjugated on the surface of one Fe_3O_4 nanoparticle is about 1. Targeting Fe_3O_4@DMSA@Ab nanoprobes against the CD20 antigen on the cell membrane can enhance the T2 MRI signal. Further investigation showed that the Fe_3O_4@DMSA@Ab nanoprobes have considerable potential to induce apoptosis in $CD20^+$ Raji cells. The possible mechanisms underlying the promotion of cell apoptosis could be related to an increase in cytosolic Ca^{2+}, ROS, and Bax/Bcl-2, and a decrease in $\Delta\Psi m$, which are initiated by the Fe_3O_4@DMSA@Ab nanoprobe-induced CD20 cluster formation. Thus, though there are still open quesions, the Fe_3O_4@DMSA@Ab nanoprobe displays great potential for future application in lymphoma treatment.

Acknowledgments

This research was supported by the National Key Research and Development Program of China (No 2017YFA0205502), the National Basic Research Program of China (973 program No 2013CB733800), National Natural Science Foundation of China (No 81571806, 81671820, 81771899), the Jiangsu Provincial Special Program of Medical Science (BL2013029), and the Fundamental Research Funds for the Central Universities.

Disclosure

The authors report no conflicts of interest in this work.

References

1. Arap W, Pasqualini R, Ruoslahti E. Cancer treatment by targeted drug delivery to tumor vasculatur in a mouse model. *Science*. 1998;279(5349):377–380.
2. Davis ME, Chen ZG, Shin DM. Nanoparticle therapeutics: an emerging treatment modality for cancer. *Nat Rev Drug Discov*. 2008;7(9):771–782.
3. Ec-Y T, Chew Y, Phipps C. A review of monoclonal antibody therapies in lymphoma. *Crit Rev Oncol/Hematol*. 2016;97:72–84.
4. Liu D, Auguste DT. Cancer targeted therapeutics: from molecules to drug delivery vehicles. *J Control Release*. 2015;219:632–643.
5. Xu X, Ho W, Zhang X, Bertrand N, Farokhzad O. Cancer nanomedicine: from targeted delivery to combination therapy. *Trends Mol Med*. 2015;21(4):223–232.
6. Scott SD. Rituximab: a new therapeutic monoclonal antibody for non-Hodgkin's lymphoma. *Cancer Pract*. 1998;6(3):195–197.
7. Mclaughlin P, Grillo-López AJ, Link BK, et al. Rituximab chimeric anti-CD20 monoclonal antibody therapy for relapsed indolent lymphoma: half of patients respond to a four-dose treatment program. *J Clin Oncol*. 1998;16(8):2825–2833.
8. Vega MI, Huerta-Yepez S, Martinez-Paniagua M, et al. Rituximab-mediated cell signaling and chemo/immuno-sensitization of drug-resistant B-NHL is independent of its Fc functions. *Clin Cancer Res*. 2009;15(21):6582–6594.
9. Simons K, Toomre D. Lipid rafts and signal transduction. *Nat Rev Mol Cell Biol*. 2000;1(1):31–39.
10. Maloney DG, Smith B, Rose A. Rituximab: mechanism of action and resistance. *Semin Oncol*. 2002;29(1):2–9.
11. Hofmeister JK, Cooney D, Coggeshall KM. Clustered CD20 induced apoptosis: src-family kinase, the proximal regulator of tyrosine phosphorylation, calcium influx, and caspase 3-dependent apoptosis. *Blood Cells Mol Dis*. 2000;26(2):133–143.
12. Popoff IJ, Savage JA, Blake J, Johnson P, Deans JP. The association between CD20 and Src-family Tyrosine kinases requires an additional factor. *Mol Immunol*. 1998;35(4):207–214.
13. Jazirehi AR, Vega MI, Bonavida B. Development of rituximab-resistant lymphoma clones with altered cell signaling and cross-resistance to chemotherapy. *Cancer Res*. 2007;67(3):1270–1281.
14. Bubien JK, Zhou LJ, Bell PD, Frizzell RA, Tedder TF. Transfection of the CD20 cell surface molecule into ectopic cell types generates a $Ca2^+$ conductance found constitutively in B lymphocytes. *J Cell Biol*. 1993;121(5):1121–1132.
15. Tan L, Lin P, Chisti MM, Rehman A, Zeng X. Real time analysis of binding between Rituximab (anti-CD20 antibody) and B lymphoma cells. *Anal Chem*. 2013;85(18):8543–8551.
16. Daniels I, Turzanski J, Haynes AP. A requirement for calcium in the caspase-independent killing of Burkitt lymphoma cell lines by Rituximab. *Br J Haematol*. 2008;142(3):394–403.
17. Jaffe ES, Harris NL, Stein H, Isaacson PG. Classification of lymphoid neoplasms: the microscope as a tool for disease discovery. *Blood*. 2008;112(12):4384–4399.
18. Chen W, Zheng R, Zhang S, et al. Cancer incidence and mortality in China, 2013. *Cancer Lett*. 2017;401(1):63–71.
19. Siegel RL, Miller KD, Jemal A. Cancer statistics, 2017. *CA Cancer J Clin*. 2017;67(1):7–30.
20. Siegel RL, Miller KD, Jemal A. Cancer statistics, 2016. *CA Cancer J Clin*. 2016;66(1):7–30.
21. Siegel RL, Miller KD, Jemal A. Cancer statistics, 2015. *CA Cancer J Clin*. 2015;65(1):5–29.
22. Ferlay J, Steliarova-Foucher E, Lortet-Tieulent J, et al. Cancer incidence and mortality patterns in Europe: estimates for 40 countries in 2012. *Eur J Cancer*. 2013;49(6):1374–1403.
23. Coiffier B. Rituximab therapy in malignant lymphoma. *Oncogene*. 2007;26(25):3603–3613.
24. Lee N, Yoo D, Ling D, Cho MH, Hyeon T, Cheon J. Iron Oxide Based Nanoparticles for Multimodal Imaging and Magnetoresponsive Therapy. *Chem Rev*. 2015;115(19):10637–10689.
25. Babes L, Denizot B, Tanguy G, Le Jeune JJ, Jallet P. Synthesis of iron oxide Nanoparticles used as MRI contrast agents: a parametric study. *J Colloid Interface Sci*. 1999;212(2):474–482.
26. Jordan A, Scholz R, Wust P, Fähling H, Roland Felix, Felix R. Magnetic fluid hyperthermia (MFH): Cancer treatment with AC magnetic field induced excitation of biocompatible superparamagnetic nanoparticles. *J Magn Magn Mater*. 1999;201(1–3):413–419.
27. Arbab AS, Bashaw LA, Miller BR, et al. Characterization of biophysical and metabolic properties of cells labeled with superparamagnetic iron oxide nanoparticles and transfection agent for cellular MR imaging. *Radiology*. 2003;229(3):838–846.
28. Janic B, Rad AM, Jordan EK, et al. Optimization and validation of FePro cell labeling method. *PLoS One*. 2009;4(6):e5873.
29. Xu C, Xu K, Gu H, et al. Dopamine as a robust anchor to immobilize functional molecules on the iron oxide shell of magnetic nanoparticles. *J Am Chem Soc*. 2004;126(32):9938–9939.

30. Huh YM, Jun YW, Song HT, et al. In vivo magnetic resonance detection of cancer by using multifunctional magnetic nanocrystals. *J Am Chem Soc*. 2005;127(35):12387–12391.
31. Lee JH, Huh YM, Jun YW, et al. Artificially engineered magnetic nanoparticles for ultra-sensitive molecular imaging. *Nat Med*. 2007;13(1):95–99.
32. Chiu GN, Edwards LA, Kapanen AI, et al. Modulation of cancer cell survival pathways using multivalent liposomal therapeutic antibody constructs. *Mol Cancer Ther*. 2007;6(3):844–855.
33. Laurent S, Forge D, Port M, et al. Magnetic iron oxide nanoparticles: synthesis, stabilization, vectorization, physicochemical characterizations, and biological applications. *Chem Rev*. 2008;108(6):2064–2110.
34. Chisolm JJ, Jjc J. Safety and efficacy of meso-2,3-dimercaptosuccinic acid (DMSA) in children with elevated blood lead concentrations. *J Toxicol Clin Toxicol*. 2000;38(4):365–375.
35. Fauconnier N, Pons JN, Roger J, Bee A. Thiolation of Maghemite Nanoparticles by Dimercaptosuccinic Acid. *J Colloid Interface Sci*. 1997;194(2):427–433.
36. Valois CR, Braz JM, Nunes ES, et al. The effect of DMSA-functionalized magnetic nanoparticles on transendothelial migration of monocytes in the murine lung via a beta2 integrin-dependent pathway. *Biomaterials*. 2010;31(2):366–374.
37. Maclaughlin CM, Parker EP, Walker GC, Wang C. Evaluation of SERS labeling of CD20 on CLL cells using optical microscopy and fluorescence flow cytometry. *Nanomedicine*. 2013;9(1):55–64.
38. Ernst JA, Li H, Kim HS, Nakamura GR, Yansura DG, Vandlen RL. Isolation and characterization of the B-cell marker CD20. *Biochemistry*. 2005;44(46):15150–15158.
39. Cragg MS, Walshe CA, Ivanov AO, Glennie MJ. The biology of CD20 and its potential as a target for mAb therapy. *Curr Dir Autoimmun*. 2005;8:140–174.
40. Xie J, Chen K, Huang J, et al. PET/NIRF/MRI triple functional iron oxide nanoparticles. *Biomaterials*. 2010;31(11):3016–3022.
41. Johnson P, Glennie M. The mechanisms of action of rituximab in the elimination of tumor cells. *Semin Oncol*. 2003;30(1):3–8.
42. Cirstoiu-Hapca A, Bossy-Nobs L, Buchegger F, Gurny R, Delie F. Differential tumor cell targeting of anti-HER2 (Herceptin) and anti-CD20 (Mabthera) coupled nanoparticles. *Int J Pharm*. 2007;331(2):190–196.
43. Roch A, Gossuin Y, Muller RN, Gillis P. Superparamagnetic colloid suspensions: Water magnetic relaxation and clustering. *J Magn Magn Mater*. 2005;293(1):532–539.
44. Berret JF, Schonbeck N, Gazeau F, et al. Controlled clustering of superparamagnetic nanoparticles using block copolymers: design of new contrast agents for magnetic resonance imaging. *J Am Chem Soc*. 2006;128(5):1755–1761.
45. Vega MI, Huerta-Yepez S, Martinez-Paniagua M, et al. Rituximab-mediated cell signaling and chemo/immuno-sensitization of drug-resistant B-NHL is independent of its Fc functions. *Clin Cancer Res*. 2009;15(21):6582–6594.
46. Gao L, Fei J, Zhao J, Li H, Cui Y, Li J. Hypocrellin-loaded gold nanocages with high two-photon efficiency for photothermal/photodynamic cancer therapy in vitro. *ACS Nano*. 2012;6(9):8030–8040.
47. Pinton P, Giorgi C, Siviero R, Zecchini E, Rizzuto R. Calcium and apoptosis: ER-mitochondria $Ca2^{+}$ transfer in the control of apoptosis. *Oncogene*. 2008;27(50):6407–6418.
48. Shan D, Ledbetter JA, Press OW. Apoptosis of malignant human B cells by ligation of CD20 with monoclonal antibodies. *Blood*. 1998;91(5):1644–1652.
49. Bubien JK, Zhou LJ, Bell PD, Frizzell RA, Tedder TF. Transfection of the CD20 cell surface molecule into ectopic cell types generates a Ca^{2+} conductance found constitutively in B lymphocytes. *J Cell Biol*. 1993;121(5):1121–1132.
50. Li H, Ayer LM, Polyak MJ, et al. The CD20 calcium channel is localized to microvilli and constitutively associated with membrane rafts: antibody binding increases the affinity of the association through an epitope-dependent cross-linking-independent mechanism. *J Biol Chem*. 2004;279(19):19893–19901.
51. Polyak MJ, Deans JP. Alanine-170 and proline-172 are critical determinants for extracellular CD20 epitopes; heterogeneity in the fine specificity of CD20 monoclonal antibodies is defined by additional requirements imposed by both amino acid sequence and quaternary structure. *Blood*. 2002;99(9):3256–3262.
52. Martindale JL, Holbrook NJ. Cellular response to oxidative stress: signaling for suicide and survival. *J Cell Physiol*. 2002;192(1):1–15.
53. Macho A, Hirsch T, Marzo I, et al. Glutathione depletion is an early and calcium elevation is a late event of thymocyte apoptosis. *J Immunol*. 1997; 158(10):4612–4619.
54. Green DR, Reed JC. Mitochondria and apoptosis. *Science*. 1998; 281(5381):1309–1312.
55. Galluzzi L, Zamzami N, de La Motte Rouge T, Lemaire C, Brenner C, Kroemer G. Methods for the assessment of mitochondrial membrane permeabilization in apoptosis. *Apoptosis*. 2007;12(5):803–813.
56. Susin SA, Zamzami N, Kroemer G. Mitochondria as regulators of apoptosis: doubt no more. *Biochim Biophys Acta*. 1998;1366(1–2):151–165.
57. Youle RJ, Strasser A. The BCL-2 protein family: opposing activities that mediate cell death. *Nat Rev Mol Cell Biol*. 2008;9(1):47–59.
58. Xiang J, Chao DT, Korsmeyer SJ. BAX-induced cell death may not require interleukin 1β-converting enzyme-like proteases. *Proc Nat Acad Sci U S A*. 1996;93(25):14559–14563.
59. Shimizu S, Narita M, Tsujimoto Y. Bcl-2 family proteins regulate the release of apoptogenic cytochrome c by the mitochondrial channel VDAC. *Nature*. 1999;399(6735):483–487.
60. Adams JM, Cory S. The Bcl-2 protein family: arbiters of cell survival. *Science*. 1998;281(5381):1322–1326.
61. Emmanouilides C, Jazirehi AR, Bonavida B. Rituximab-mediated sensitization of B-non-Hodgkin's lymphoma (NHL) to cytotoxicity induced by paclitaxel, gemcitabine, and vinorelbine. *Cancer Biother Radiopharm*. 2002;17(6):621–630.
62. Cartron G, Watier H, Golay J, Solal-Celigny P. From the bench to the bedside: ways to improve rituximab efficacy. *Blood*. 2004; 104(9):2635–2642.
63. Jazirehi AR, Bonavida B. Cellular and molecular signal transduction pathways modulated by rituximab (rituxan, anti-CD20 mAb) in non-Hodgkin's lymphoma: implications in chemosensitization and therapeutic intervention. *Oncogene*. 2005;24(13):2121–2143.
64. Lalatonne Y, Richardi J, Pileni MP. Van der Waals versus dipolar forces controlling mesoscopic organizations of magnetic nanocrystals. *Nat Mater*. 2004;3(2):121–125.
65. Dobson J. Remote control of cellular behaviour with magnetic nanoparticles. *Nat Nanotechnol*. 2008;3(3):139–143.